isvr Institute of Sound and Vibration Research

Equipment Isolation of a SDOF System with an Inertial Actuator using Feedback Control Strategies – Part II: Experiment

L, Benassi, S.J. Elliott and P. Gardonio

ISVR Technical Memorandum No 896

October 2002

University of Southampton

SCIENTIFIC PUBLICATIONS BY THE ISVR

Technical Reports are published to promote timely dissemination of research results by ISVR personnel. This medium permits more detailed presentation than is usually acceptable for scientific journals. Responsibility for both the content and any opinions expressed rests entirely with the author(s).

Technical Memoranda are produced to enable the early or preliminary release of information by ISVR personnel where such release is deemed to the appropriate. Information contained in these memoranda may be incomplete, or form part of a continuing programme; this should be borne in mind when using or quoting from these documents.

Contract Reports are produced to record the results of scientific work carried out for sponsors, under contract. The ISVR treats these reports as confidential to sponsors and does not make them available for general circulation. Individual sponsors may, however, authorize subsequent release of the material.

UNIVERSITY OF SOUTHAMPTON

INSTITUTE OF SOUND AND VIBRATION RESEARCH

SIGNAL PROCESSING AND CONTROL GROUP

Equipment Isolation of a SDOF System with an Inertial Actuator using Feedback Control Strategies - Part II: Experiment

by

L. Benassi, S. J. Elliott and P. Gardonio

ISVR Technical Memorandum No. 896

October 2002

Authorised for issue by
Prof S J Elliott
Group Chairman

ABSTRACT

Vibration isolators are required to protect a delicate piece of equipment from the vibration of a structure to which it is attached. In this report the experimental work conducted to evaluate the active control of the single degree of freedom system is described. The overall aim of this report is to compare theoretical analysis and experimental results to verify the conclusions on control strategies discussed in the previous work. In order to achieve this, experiments were conducted using a SDOF system set on a flexible foundation. Open and closed loop responses were measured with the feedback control strategies applied.

It was confirmed that from a stability point of view, the force and velocity feedback control scheme does not guarantee a good stability margin at low frequency. This is especially true when the outer velocity gain is increased. On the other hand, from a performance point of view, this scheme offers very good results using lower power than the other schemes.

When an integrator is added to the system, the overall system significantly improves its stability characteristics. On the other hand, if high performance is needed, very high gains are necessary and therefore a lot of power is consumed.

The idea then to use a phase-lag compensator within the inner loop and a velocity feedback outer loop seems to be very attractive. In fact, good stability margins can be achieved, and very good performance was obtained.

TABLE OF CONTENTS

1. INTRODUCTION

Isolating a piece of delicate equipment from the vibration of a base structure is of practical importance in various engineering fields. Examples are the vibration isolation of the instrument boxes in an aircraft and the isolation of telescopes on satellites. An active isolation system can be implemented over a broad frequency band using different feedback control strategies. This report investigates the experimental work on the active isolation of a rigid piece of equipment structure from the vibration of a flexible base structure. The objective is to study the performance and control stability issues associated with the active vibration isolation system. Particular emphasis is placed on the isolation of low frequency vibration (0~50Hz), in which the equipment resonance lies and for which the mounts can be assumed to behave as lumped springs and dampers. A theoretical model was derived in a previous work (Benassi, *et al.*, 2002a, b and c) using the impedance method to investigate the dynamic behaviour of the system. Also, the effect of electronic components as potential cause of low and high frequency instability was investigated by Ananthaganeshan *et al.* (2001), Ren *et al.* (1997) and Benassi *et al.* (2002a). Another objective of this work is then to compare those theoretical findings with the experiments.

A description of the experimental apparatus and implementation of the active vibration isolation system is given in section 2, and the theoretical model is validated experimentally in section 3. Control stability of the active isolator is evaluated experimentally for each control strategy and the performances of single-channel and multi-channel (when multiple sensors are contributing to the control strategy) active vibration control systems with a rigid equipment structure are then discussed. Section 4 summarizes the conclusions.

2. DESCRIPTION OF THE EXPERIMENTAL SET-UP

In this section the equipment and set-up used to perform the experiments are described. Figure 1 shows the active mount system used in the experimental work. It consists of an aluminium rigid mass, two mounts placed symmetrically underneath the aluminium mass and one electromagnetic shaker to produce the control force. The aluminium plate had been previously shown (Serrand, 1998) to behave as a rigid mass up to 1000 Hz, which is well above the maximum frequency of interest in this experimental study. The shaker is placed on top of the mass and its weight is held by a suspension system. This arrangement is necessary in order for the shaker to behave as an inertial actuator. This system is attached to a flexible plate made of steel. Accelerometers and force gauges are used as sensors.

The piece of equipment

The receiving body (simulating a delicate piece of equipment) is composed of a thick aluminium plate. The receiver behaves as a rigid mass in the frequency range 0-1000 Hz. At 1000 Hz, the passive isolation provides such good performances and the axial plate motion is so small that any little errors in the equipment rigidity assumption would bring no change to the assessment of the controller performances. The receiver is thus considered fully rigid in the frequency range of analysis. Further details are given in Table A1 in Appendix A.

The passive mounts

The passive isolation consists of a pair of rings of rubber each of which is mounted between two aluminium discs. The top disc is rigidly connected to the piece of equipment while the bottom disc can be bolted to the vibrating base structure. The passive parts of both mounts were assumed to have the same mechanical properties. Figure 2 shows a schematic diagram of the system and further details are given in Table A2 and Table A3 in Appendix A.

The inertial actuator

The active force is provided by an electro-mechanic shaker fixed on top of the piece of equipment. A single shaker is placed in the middle of the equipment structure so that the shaker itself acts as the inertial mass, as illustrated in Figure 1. The mechanical properties of the actuator are given in Table A6 in Appendix A.

Its main components comprise a coil moving in the steady magnetic field of a permanent magnet. The force generated and transmitted to the piece of equipment is proportional to the product of the instantaneous current in the coil and the magnetic flux density. The shaker can only generate axial forces and therefore only the axial motion can be entirely controlled, since the mass is supposed to be perfectly rigid in the frequency range of interest. A single channel system can thus be regarded as controlling the heave mode (vertical translation) of the rigid mass on the mounts. Since the shaker and rubber mounts are symmetrically placed with respect to the mass centre of the aluminium plate, it is therefore possible to treat the system as a SDOF system

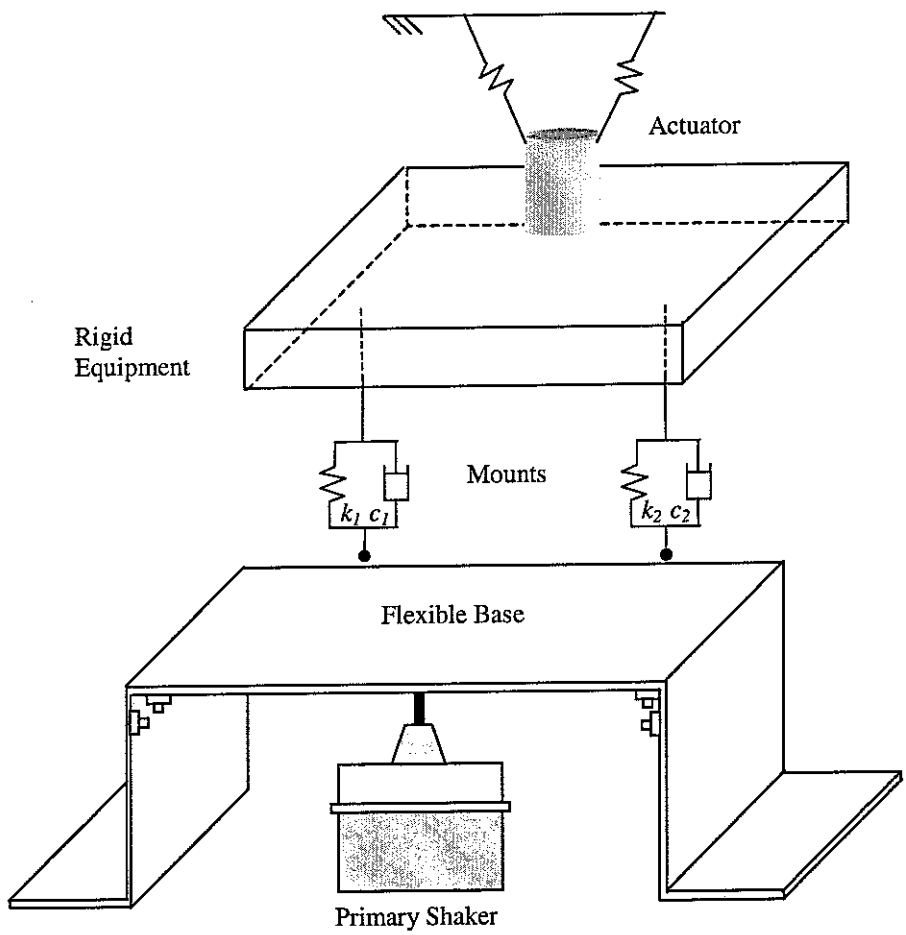

Figure 1. *Schematic diagram of a two mount active isolation system with a rigid equipment structure on a flexible base.*

The vibrating plate

The third main element of the base vibration isolation problem is the flexible base on which the disturbances are generated. A steel plate clamped on two opposite edges and free on the two others was designed to model experimentally a realistic vibrating base. The requirements are:

1. to use a simple design, enabling a relatively simple theoretical model
2. to design a base with a sufficient static rigidity to support the equipment
3. to get a large enough vibration on the base to drive the isolator so that the velocity response signals on the top of the receiving equipment can be easily measured.

The requirement of a good dynamic range of plate vibration was motivated by the high expected efficiency of the passive isolation of the mounts. A low axial stiffness of the passive mounts provides an efficient attenuation of the axial vibration at high frequency. To be able to assess the effectiveness of an active isolation in a wider frequency range than in the vicinity of the axial equipment rigid body modes, a strong plate motion is necessary in order to recover a measurable vibration signal on the top of the equipment that is not too corrupted by measurement noise.

The choice of a clamped-free-clamped-free plate was made in the attempt to fulfil all these requirements (Leissa, 1969). A complete analysis of the design and construction of the vibrating plate can be found in Gardonio's work (1996, 1997a and 1997b). A Matlab program of the coupled dynamics was written as the basis for all the theoretical simulations.

The first plate resonance lies around 33 Hz and the modal damping was assumed to be 1% to better fit the experimental results.

Appendix A lists the first nine modes of the base supporting plate. The experimental modal frequencies listed in Table A5 are lower than those predicted by the theoretical model. This can be explained by the imperfections of the clamping conditions. The strengthening pieces connecting the plate to the ticker vertical supports prevent almost any bending of the plate at the clamped edges at low frequencies in one sense of rotation (downwards) but not in the other (upwards). The second imperfection lies in the fact that the vertical supports are not absolutely rigid especially at low frequency. This acts to reduce the stiffness of the system, therefore shifting down the natural frequencies, particularly those for the lower order modes.

The main differences between model and experiments at higher frequencies arise as the spacing between two consecutive bolts connecting the plate to the strengthening pieces is no longer negligible compared to the wavelength of the propagating wave. The junction between the strengthening pieces and the plate itself can thus not be regarded as a perfectly clamped junction. Secondly, the system dynamics will become affected by small structural details as the frequency increases, since the wavelength will get shorter.
Further details about this topic are given in Serrand (1998).

The primary shaker

As shown in Figure 1, one shaker was used as primary force to drive the system. It was placed in the centre of the flexible base and it was driven by the output of the signal generator within the FFT analyser. Its main properties are described in Table A7.
The foundation is not only moved by the shaker but also by the two cylindrical mounts as they are stretched and compressed. These two forces couple the dynamics of the plate and the isolator.

Sensors

Before any control technique is applied, identification of the experimental system and the characteristics of each instrument used are important.
The force generated by the primary shaker is monitored using a piezoelectric force gauge (B&K type 8200) whose bottom side is bolted to the shaker and top side is stuck to the plate (Figure 2). The acceleration of the centre of the piece of equipment is measured at one point on the equipment using a piezoelectric accelerometer (B&K type 4375) monitoring the vertical motion. The total transmitted force to the equipment is measured by a second piezoelectric force gauge (B&K type 8200) whose top side is bolted to the secondary shaker (the inertial actuator) and bottom side is bolted to the centre of the aluminium mass. A complete list of the equipment used is given in Appendix A, Table A9.

After having analysed the different elements constituting the parts of the isolation problem, it is now possible to investigate the dynamics of the complete system when different control strategies are applied to the laboratory set-up shown in Figure 3 and Figure 4. This will be achieved by measuring the rigid mass response to the shaker excitation moving the flexible plate underneath.

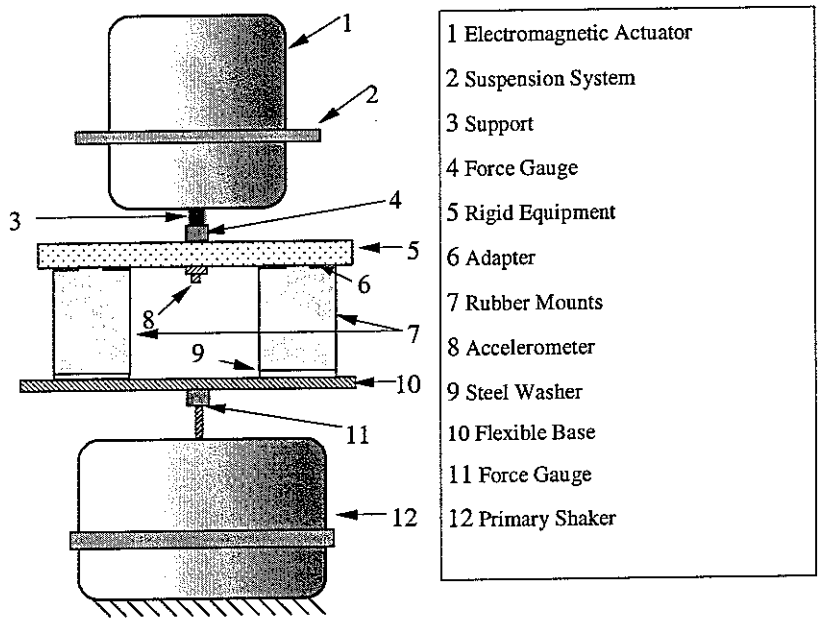

Figure 2. *Schematic diagram of the location of sensors and actuator within the experimental set-up.*

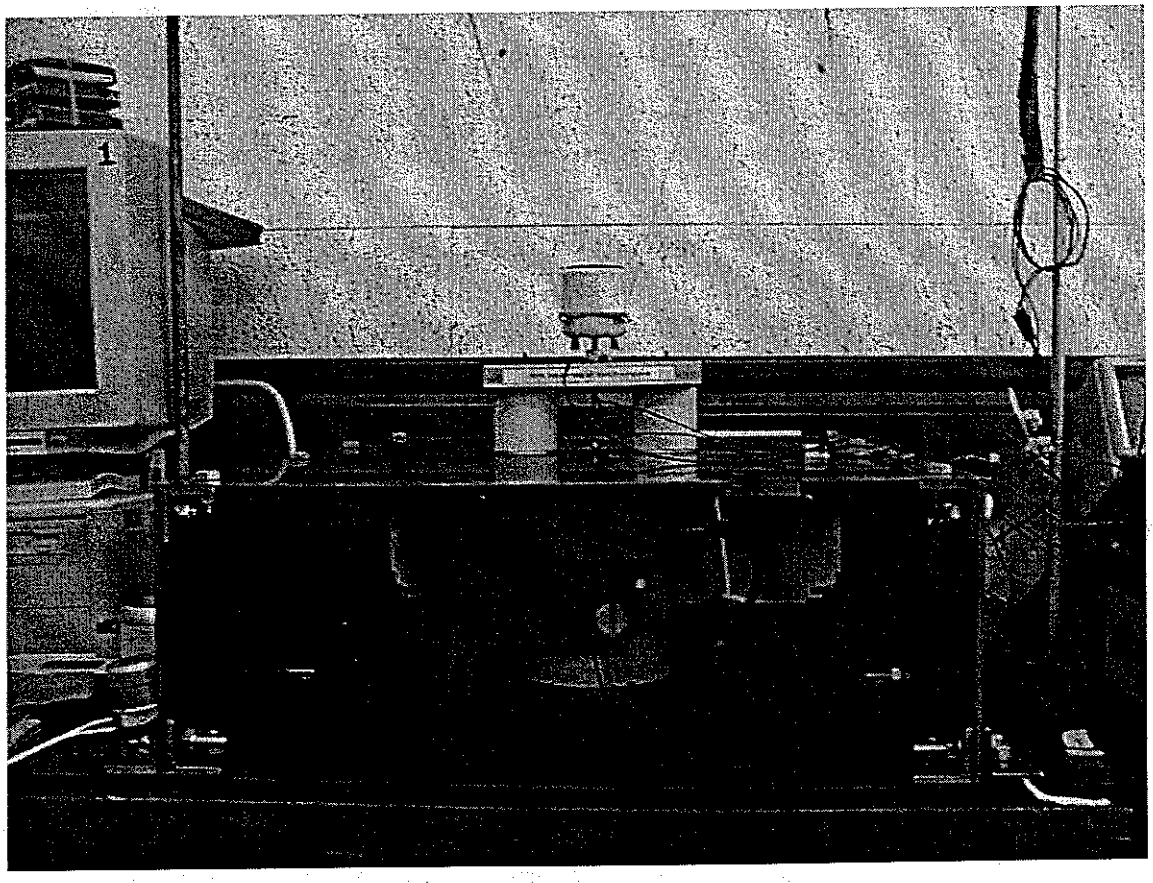

Figure 3. *Image of the experimental set-up.*

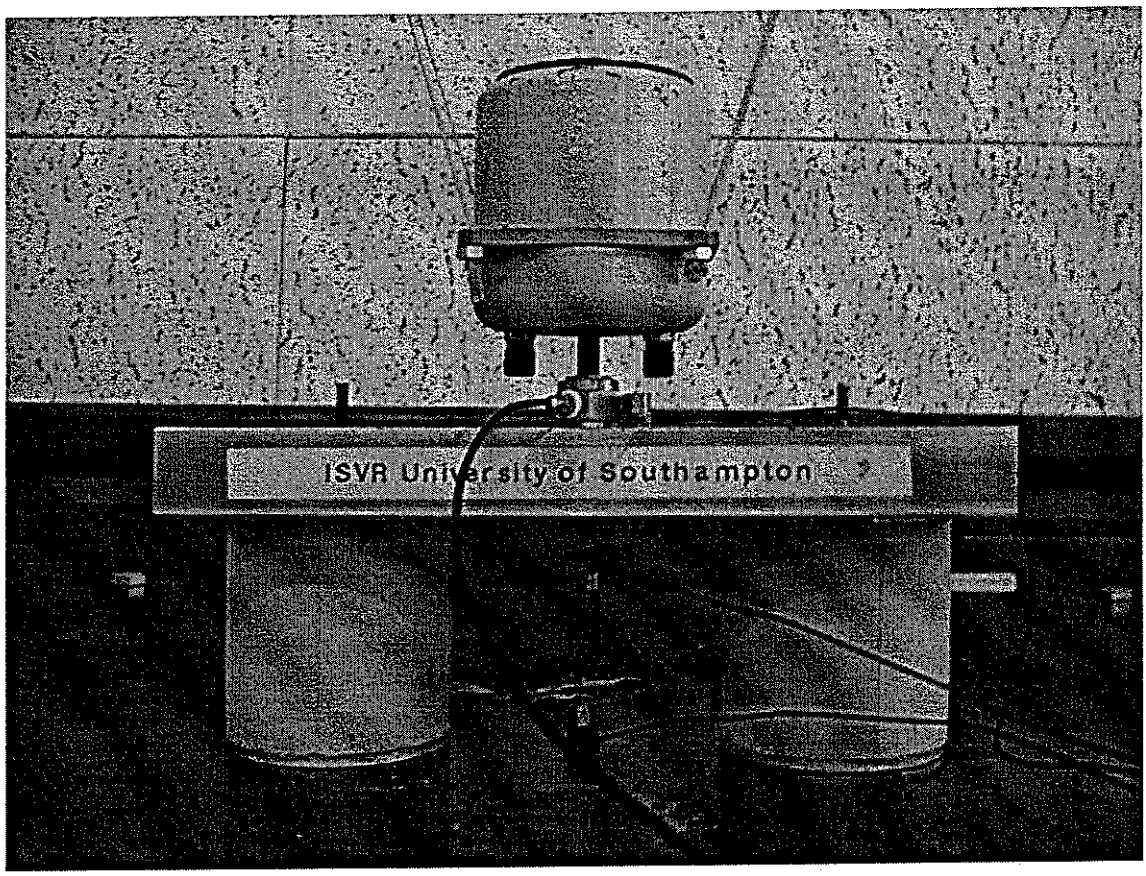

Figure 4. *Image of the core of the experimental set-up, which consists of the piece of equipment, which is mounted on top of passive rubber rings. The suspended inertial actuator is connected to the receiver and a force gauge in between measures the total transmitted force to the equipment.*

3. EXPERIMENTAL IMPLEMENTATION OF THE CONTROL STRATEGIES

In order to approximate a single degree of freedom isolation problem, the shaker is located under the centre of the flexible plate which is the centre of symmetry of the foundation. The excitation is thus on a nodal line of all the modes whose shapes are not symmetrical compared to this centre. They are then not excited and do not contribute to the plate motion. Therefore, provided the centre of the rigid mass of the isolation system is exactly at the vertical of the plate centre, both rubber mounts undergo the same displacement and the system tends to a single degree of freedom isolation problem.

Setting apart the issue of how to position the primary and secondary shakers at the exact locations, such an idealization is obviously not perfect. Neither the rubber rings nor the shakers have a point connection with the plate. For instance, the surface at the bottom of the mounts attached to the foundations is rather large. The out of plane displacement of the support may therefore generate moments and displacements in torsion at the bottom of the mounts thus exciting the mass in transversal and longitudinal directions. However, because of the symmetry of the plate modes involved, these components act in opposite directions on the two mounts and cancel out. This effect is therefore unlikely to be significant.

Another effect that was present in the measurements was that the resonance frequency of the inertial actuator-dominated mode was a little greater than the predicted value. This was due to the suspension system, which in theory had to hold the actuator mass, but in practice it added a small contribution to the stiffness of the inertial actuator. This property of the system was detected by measuring the system dynamic response using different suspension systems. In order to reduce this effect, both rubber bands and steel wires with very soft springs were tested. It was decided to use the latter solution because it showed a better linear behaviour.

Before conducting the experiments, the transfer functions of all the mechanical and electronic components were measured, and their phase characteristics were accurately analysed for a better interpretation of the experimental measurements. The smallest frequency increment possible was chosen and the gathered data was not treated in the first place. Then some minor post-processing was performed on the data, as it will be presented in this report.

Figure 5 shows a comparison between the measured plant response from primary force to equipment velocity and the simulation. The inertial actuator-dominated resonance is at about 10 Hz. It can be noted that the real system appears more damped. At about 22 Hz the simulated equipment resonance shows a very good agreement with the experimental data, both in terms of magnitude and phase. The first flexible plate modal frequency which is visible from the accelerometer placed at the centre of the set-up is at about 40 Hz and its discrepancy with the simulation was explained in the previous section. Very good coherence was obtained during all the experimental measurements, and Figure 6 shows one example of it, taken from a force and velocity feedback scheme. At frequencies higher than 5 Hz the coherence is almost always unity, and at frequencies lower than 5 Hz the really poor coherence indicates that the experimental measurements have no physical meaning at such low frequencies.

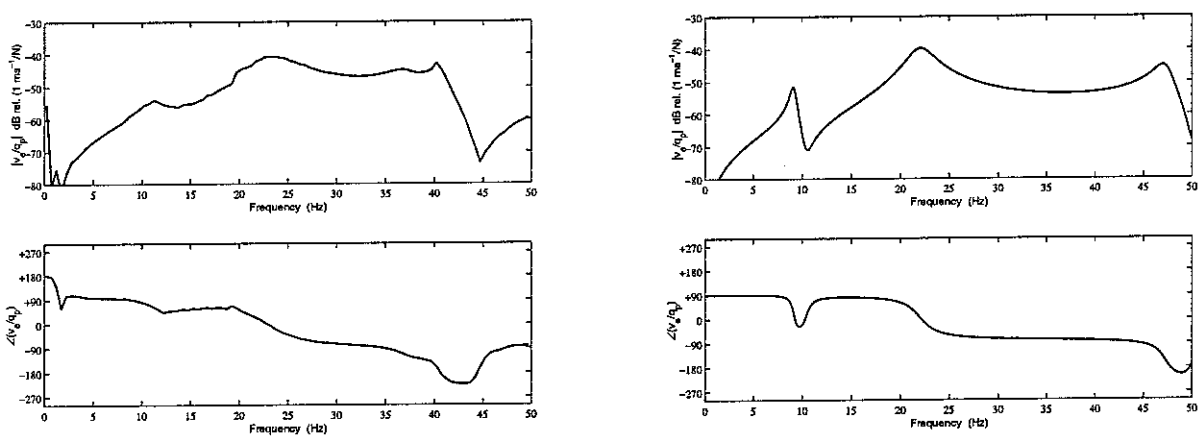

Figure 5. *Measured(left) and simulated (right) plant response from primary force to equipment velocity.*

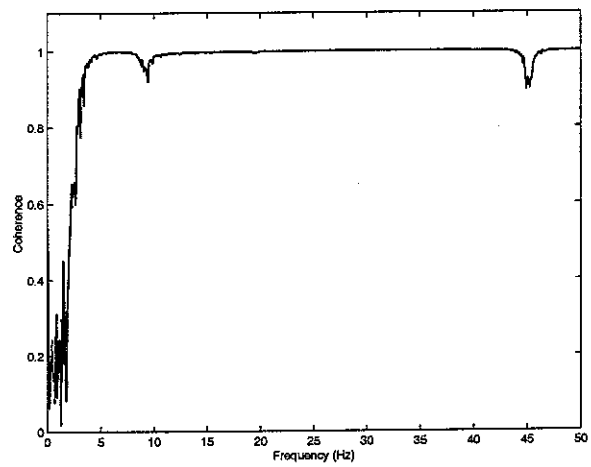

Figure 6. *Example of measured coherence of the system.*

3.1 Velocity feedback control

In this experiment, in order to evaluate the stability properties of the closed loop system by analysing the behaviour of the open loop system, white noise from an FFT analyser (Advantest R9211C) was used to drive the secondary shaker (inertial actuator). This signal was also connected to channel A of the analyser. When the equipment structure was excited, the acceleration signal at centre of the piece of equipment was measured via an accelerometer (B&K type 4375). The acceleration signal was then passed to a general signal conditioner (B&K type 2635) and converted to a velocity signal by an integrated module inside the signal conditioner. The integrator was operated in conjunction with a high-pass filter, whose cut-off frequency was preset to be 1 Hz. Finally the velocity signal was connected into channel B of the analyser to measure the frequency response function of the absolute equipment velocity per unit secondary force. Figure 7 shows a practical implementation of the experimental set-up, and Figure 9 (left) shows the Nyquist plot obtained from this measurement. The vectors of the measured signals contain 801 values each, and they cover the frequency range 0-50 Hz.

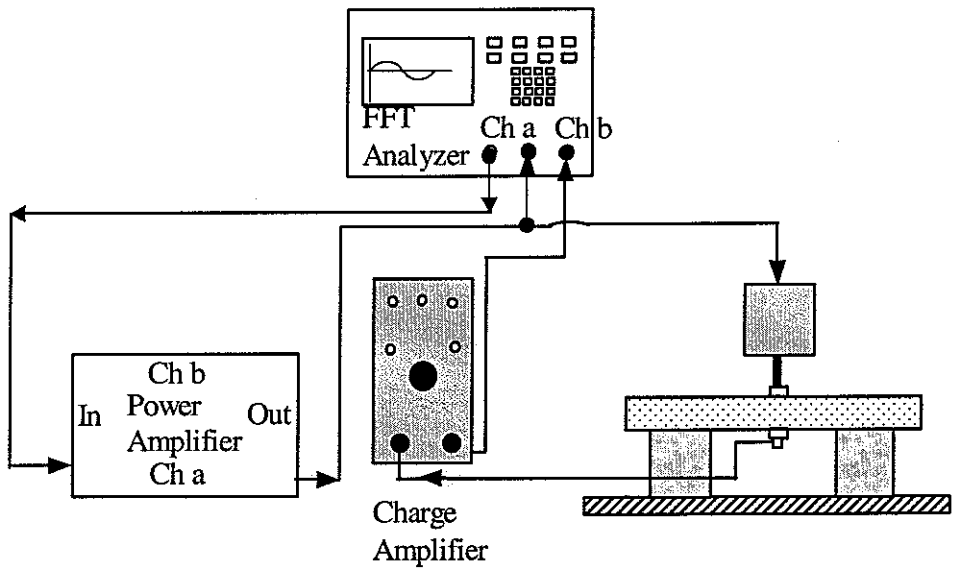

Figure 7. *Practical configuration in order to determine the equipment velocity per unit secondary excitation.*

In order to evaluate the performance of the velocity feedback strategy described in Benassi *et al.* (2002a), Section 2.1, the same FFT analyser (Advantest R9211C) was used to

measure the velocity response of the piece of equipment as well as generate the white noise signal. The white noise signal drove the primary shaker to excite the flexible base, and the excitation force signal was measured by a force transducer (B&K type 8200) connected to channel A of the analyser. When the equipment structure was excited, the acceleration signal at the centre of the piece of equipment was measured via an accelerometer (B&K type 4375). The acceleration signal was then passed to a general signal conditioner (B&K type 2635) and converted to a velocity signal by an integrated module inside the signal conditioner. The integrator was operated in conjunction with a high-pass filter, whose cut-off frequency was preset to be 1 Hz. Finally, the velocity signal was connected into channel B of the analyser to measure the frequency response function of the absolute equipment velocity per unit excitation force. A built-in filter in the analyser was employed to reduce aliasing. Figure 8 shows a practical implementation of the experimental set-up, and Figure 9 (right) shows the experimental results.

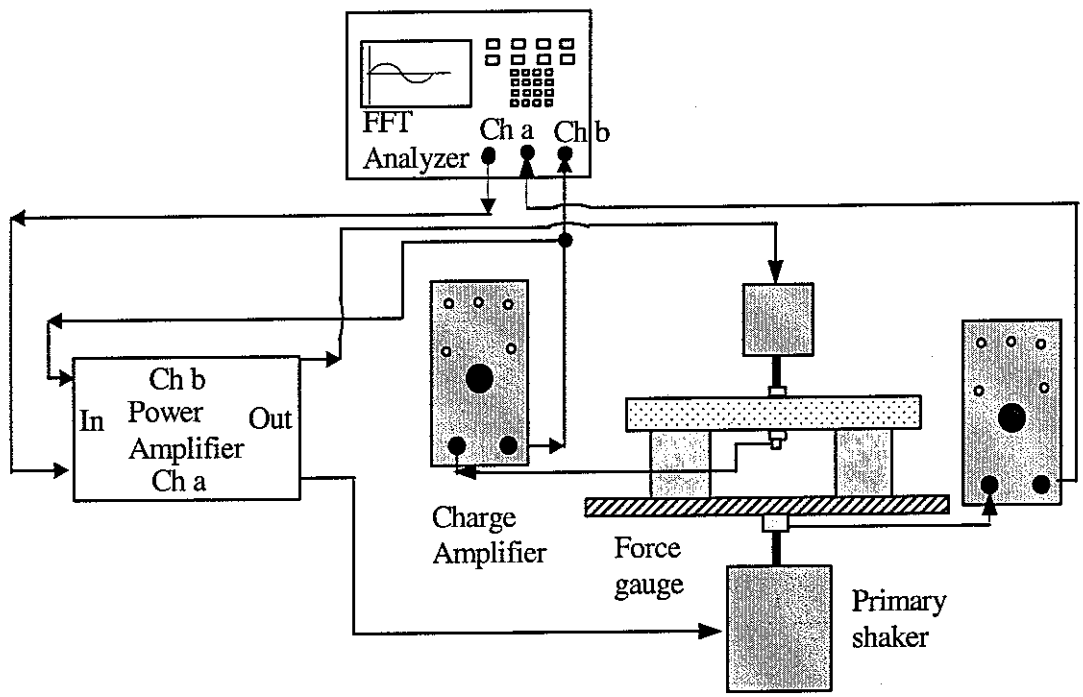

Figure 8. *Practical configuration in order to determine the equipment velocity per unit primary excitation.*

The measured plant response, from secondary shaker input to integrated accelerometer output, for the active isolation system with the inertial actuator is shown in Figure 9 (left),

which is similar to the simulated response shown in Figure 11 (left), except for a more pronounced behaviour of the flexible base in the measured data. There is no primary disturbance arising from the base support, and the loop on the left hand side of the Nyquist plot, which is due to the actuator resonance, gives rise to disturbance enhancement if the feedback gain is low enough for the system to be stable and is also the cause of instability at higher feedback gains.

The spectrum of the measured equipment velocity, normalized by the primary force, is shown in Figure 9 (right) with no control and with three values of feedback gain. It can be seen that attenuation of the vibration at the mounted equipment resonance, which has a frequency of about 23 Hz, can be achieved using this arrangement, but that some enhancement of the disturbance at the actuator resonance frequency (11 Hz) then occurs, as expected. This enhancement increases rapidly if the feedback gain is further increased until the system becomes unstable. Almost no attenuation was observed in the higher frequency base resonances with this system. The results of the computer simulations of the inertial control system are shown in Figure 11 (right) and these are again comparable with the measurements. The maximum measured attenuation is about 12 dB, compared with a predicted value for this configuration of about 13 dB. In the simulations, at high gains, the actuator resonance is sharper than in the measurements and although attenuation is present as well in the simulated performance at frequencies greater than 30 Hz, in the measurements this behaviour was more pronounced.

The resonance at about 40 Hz (Table A8) is the first flexible plate mode that can be measured with this configuration. It can be noted that the control strategy is very effective within the equipment frequency range and effective in a minor way at higher frequencies. In other words, active vibration isolation is achieved, since "the frequency response plot of the transfer function shows that damping values sufficient to control the resonance have no adverse effect on high frequency isolation" (Karnopp, 1995).

Figure 9 shows the untreated data as it was gathered, comprising 801 points in the range 0-50 Hz. While measuring, 25 averages were taken in the frequency domain by the analyser. For a clearer presentation of the experimental results, the collected data was averaged every 8 data points and the results are shown in Figure 10. It was decided to apply this simple treatment to all the data collected and present the experimental results in this form.

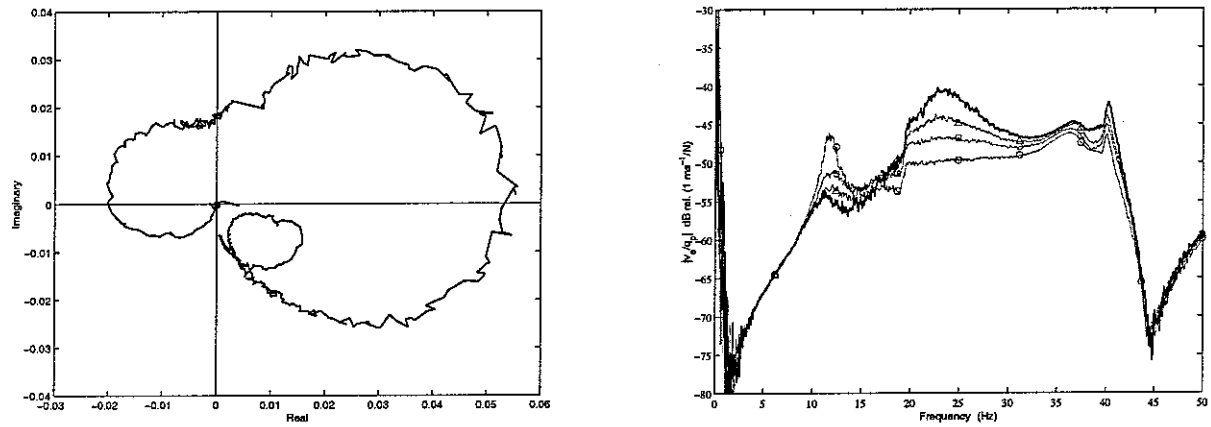

Figure 9. *Left: Nyquist plot of the untreated measured plant response from secondary shaker input to integrated accelerometer output. Right: untreated measured velocity of the equipment per unit primary excitation. Results are shown for the passive system (control off, solid line) and for three values of feedback gain (faint lines): h_v =8 (triangle), h_v = 15 (square), and h_v = 22 (circle). For gains greater than 22 the system was unstable.*

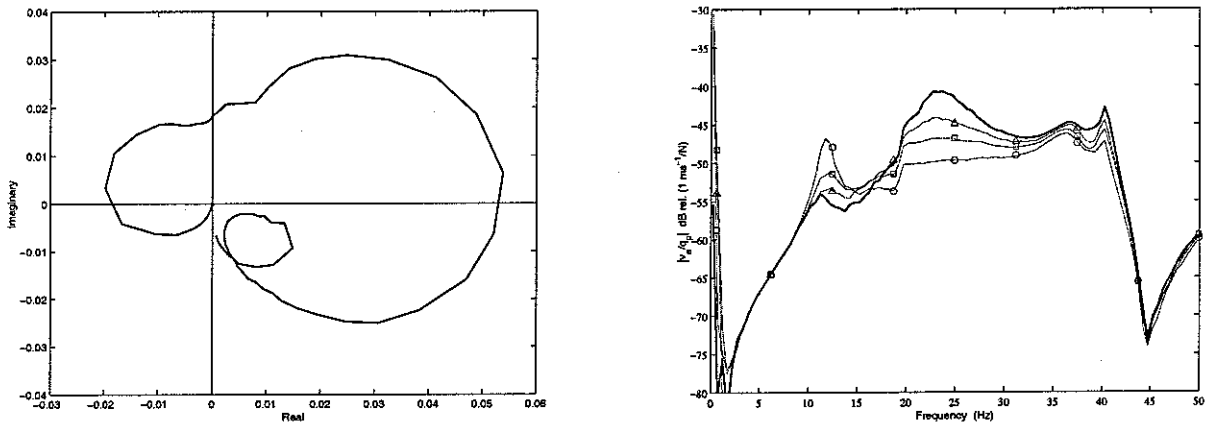

Figure 10. *Left: Nyquist plot of the treated measured plant response from secondary shaker input to integrated accelerometer output. Right: treated measured velocity of the equipment per unit primary excitation. Results are shown for the passive system (control off, solid line) and for three values of feedback gain (faint lines): h_v =8 (triangle), h_v = 15 (square), and h_v = 22 (circle). For gains greater than 22 the system was unstable.*

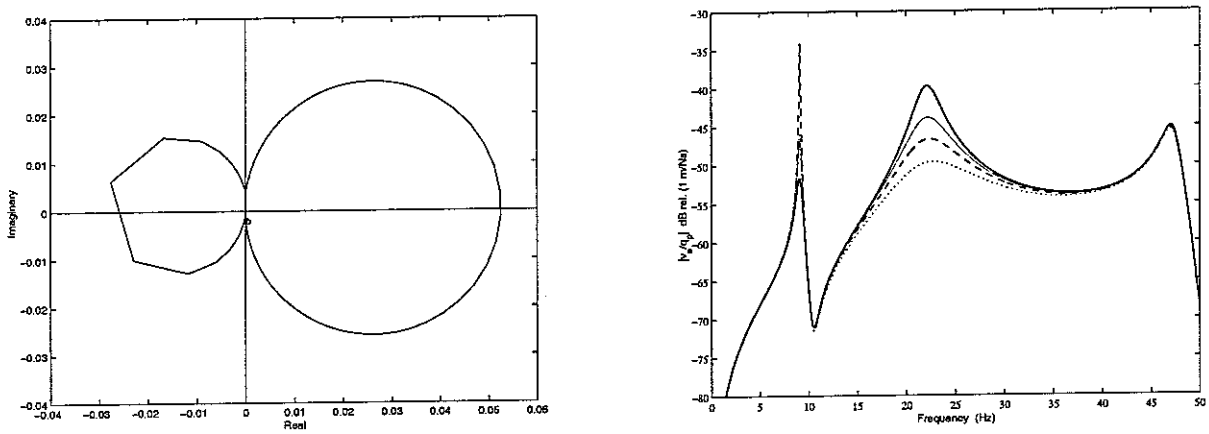

Figure 11. *Left: Nyquist plot of the simulated plant response from secondary shaker input to integrated accelerometer output. Right: simulated velocity of the equipment per unit primary excitation. Results are shown for the passive system (control off, solid line) and for three values of feedback gain:* h_v *=8 (faint line),* h_v *= 15 (dashed line), and* h_v *= 22 (dotted line). For gains greater than 25 the simulated system was unstable.*

Also, the following considerations were drawn while working on this first control strategy, but they were then applied to all the other experiments.

Due to the imperfect operation of the electrical equipment and low coherence suffered at low frequencies, the corresponding plots from the experiment show very high values at very low frequencies. Smooth curves at low frequencies are observed in the simulation since perfect operation of the electrical equipment is assumed.

Also, in the simulations, the feedback control gain relating the secondary force to the control velocity in unit of Ns/m must account for the different gains used in the experimental feedback loop, which comprises the charge amplifier gain, the power amplifier gain, and the sensitivity of the actuator. The sensitivity of the accelerometer is directly taken into account by the charge amplifier. Therefore, feedback control gain values were measured from the different components of the experimental set-up and modelled in the simulation for comparison purposes.

The open and closed loop frequency response functions for velocity feedback control with 1 Hz and 10 Hz charge amplifier cut-off frequency were obtained keeping all the other conditions unchanged. It was seen that when the amplifier cut-off frequency within the charge amplifier is increased from 1 Hz to 10 Hz the maximum attainable gain reduces considerably.

3.2 Integrated velocity feedback control

In this experiment, the same configurations as in section 3.1 were used in order to evaluate the stability properties and the performance of the closed loop system. The only difference was an ISVR-built integrator (R = 470 kΩ, C = 2.2 μF), which was used as a controller in the feedback loop before the power amplifier. This allowed the equipment velocity signal to be connected to the FFT analyser for measurement purposes, and also to be integrated within the feedback leg of the experimental set-up.

The measured plant response, from secondary shaker input to integrated velocity output, for the active isolation system with the inertial actuator is shown in Figure 12 (left), which matches to the simulated response shown in Figure 13 (left), except for a more pronounced behaviour of the flexible base. Even in this case, there is no primary disturbance arising from the base support. Compared to the previous case, the Nyquist plot appears rotated by 90° clock-wise. This is due to the effect of the integrator in the controller. Also, the presence of low frequency causes of instability can be seen. This was expected, and actually predicted in Benassi *et al.* (2002a). The spectrum of the measured equipment velocity, normalized by the primary force, is shown in Figure 12 (right) with no control and with three values of feedback gain. It can be seen that attenuation of the vibration at the mounted equipment resonance can be achieved using this arrangement, but that some enhancement of the disturbance at the actuator resonance frequency then occurs. This is due to the non-perfect characteristics of the electronic components that were used during the experiments. This enhancement increases rapidly if the feedback gain is further increased until the system becomes unstable. The results of the computer simulations of the inertial control system with an ideal integrator show good agreement with the measurements (Figure 13, right). The maximum measured attenuation is about 8 dB and the tendency of separating the first two resonances apart when the gain is increased is clearly observed and predicted by the simulations.

In summary, integrated velocity feedback control is unconditionally stable for an ideal system, while it is conditionally stable for real systems. This was shown both including in the simulations the effect of the electronic components and also experimentally. The performance of an ideal integrated velocity feedback controller is good within a considerable frequency range, but unfortunately high gains may be needed to obtain

substantial attenuation and this is clearly a limit because in real systems high gains do not guarantee stability.

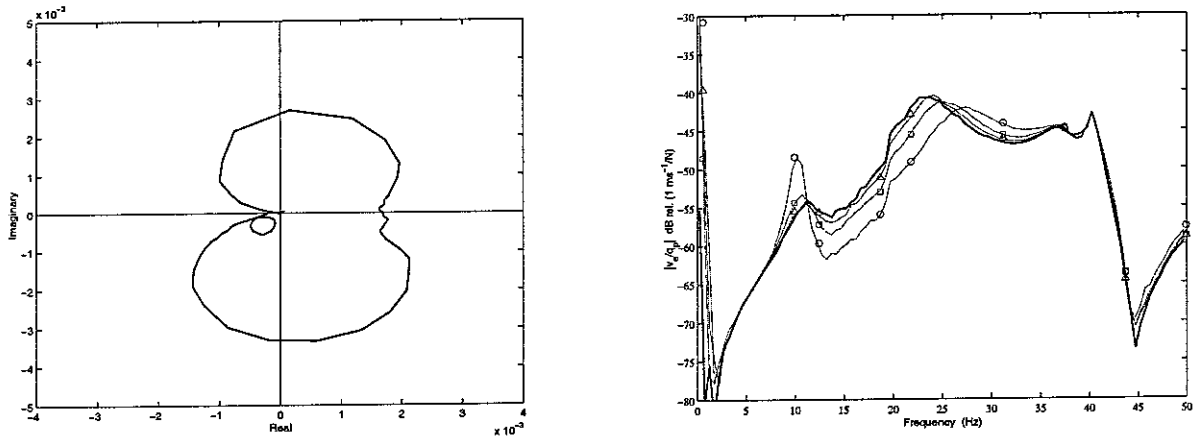

Figure 12. *Left: Nyquist plot of the treated measured plant response from secondary shaker input to integrated accelerometer output when the controller is an integrator. Right: treated measured velocity of the equipment per unit primary excitation. Results are shown for the passive system (control off, solid line) and for three values of feedback gain (faint lines): h_{iv} =6 (triangle), h_{iv} = 10 (square), and h_{iv} = 20 (circle). For gains greater than 20 the system was unstable.*

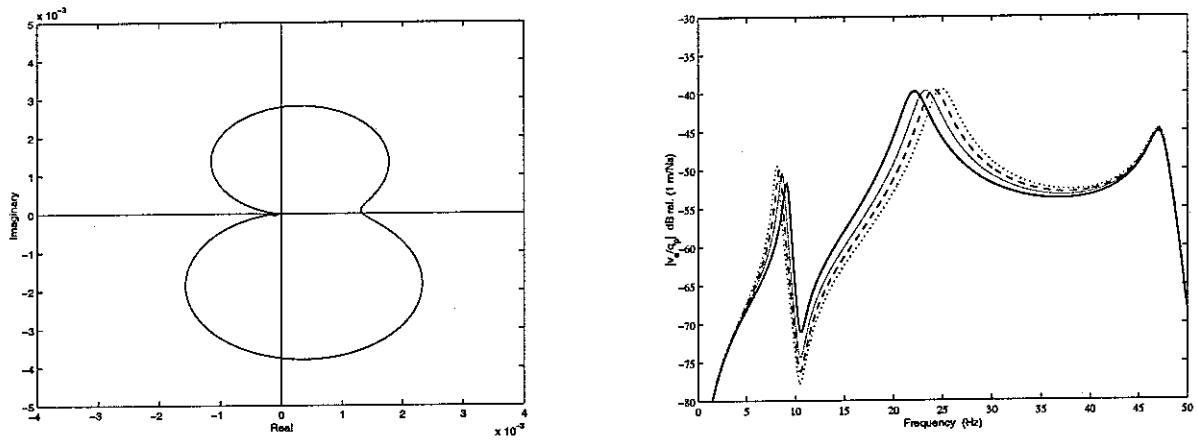

Figure 13. *Left: Nyquist plot of the simulated plant response from secondary shaker input to integrated accelerometer output when the controller is an integrator. Right: simulated velocity of the equipment per unit primary excitation. Results are shown for the passive system (control off, solid line) and for three values of feedback gain: h_{iv} =6 (faint line), h_{iv} = 10 (dashed line), and h_{iv} = 20 (dotted line). The ideal system is unconditionally stable.*

3.3 Force feedback control

In this experiment, in order to evaluate the stability properties of the closed loop system by analysing the behaviour of the open loop system, white noise form the FFT analyser was used to drive the secondary shaker (inertial actuator). This signal was also connected to channel A of the analyser. When the equipment structure was excited, the force signal between the inertial actuator and the piece of equipment was measured via a force gauge of the same kind as that one used to measure the primary force. The force signal was then passed to a general signal conditioner (B&K type 2635). Finally the force signal, which is in fact the total transmitted force to the equipment, was connected into channel B of the analyser to measure the frequency response function of the total transmitted force per unit secondary force. Figure 14 shows a practical implementation of the experimental set-up, and Figure 17 (left) shows the Nyquist plot obtained from this measurement.

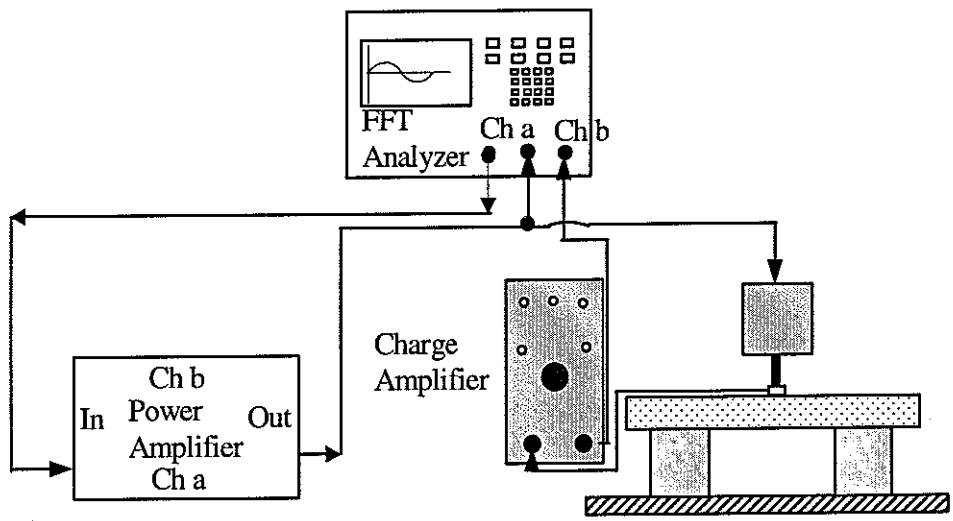

Figure 14. *Practical configuration in order to determine the total transmitted force per unit secondary excitation.*

In order to evaluate the performance of the strategy described in Benassi *et al.* (2002b and 2002c), the same FFT analyser was used to measure the velocity response of the piece of equipment as well as generate the white noise signal. The white noise signal drove the primary shaker to excite the flexible base, and the excitation force signal was measured by a force transducer which was also connected to channel A of the analyser. When the equipment structure was excited, the acceleration signal at the centre of the piece of

equipment was measured via an accelerometer. The acceleration signal was then passed to a general signal conditioner and converted to a velocity signal similarly to the previous cases. Finally, the velocity signal was connected into channel B of the analyser to measure the frequency response function of the absolute equipment velocity per unit excitation force. A built-in filter in the analyser was employed to reduce aliasing. Unlike the previous cases however, the feedback control strategy is based on the measurement of the total transmitted force to the equipment. To implement this feature, the force gauge between the inertial actuator and the piece of equipment measures the total transmitted force, whose signal then passes to a signal conditioner. The output of the signal conditioner becomes the input to the power amplifier which in fact acts as the gain module within the feedback leg. The amplified signal is then connected to the secondary shaker (the inertial actuator) for actuation. Figure 15 shows a practical implementation of the experimental set-up, and Figure 17 (right) shows the experimental results.

Figure 16 shows the total transmitted force to the equipment per unit equipment velocity. It can be noted that when the force feedback gain in increased, the inertial actuator resonance is pushed to lower frequencies. As expected, the low coherence at the first flexible base resonance causes the data to be not well defined.

The measured plant response, from secondary shaker input to total transmitted force, for the active isolation system with the inertial actuator is shown in Figure 17 (left), which is similar to the simulated response shown in Figure 18 (left). Also in this case, there is no primary disturbance arising from the base support. The stability analysis of such a system plays an important role in the discussion about whether force and velocity feedback control is a good solution to the equipment isolation problem. At low frequency, as predicted by the simulations, the Nyquist plot lies very close to the critical point and therefore instability is likely to happen when the gain is increased.

The spectrum of the measured equipment velocity, normalized by the primary force, is shown in Figure 17 (right) with no control and with three values of feedback gain. It can be seen that enhancement of the vibration at the mounted equipment resonance is experienced using this arrangement, as expected.

An important aspect is that, when the gain h_f increases, the actuator resonance is shifted to lower frequencies, while its magnitude increases, getting closer to the unstable region. This was described in theory by Benassi *et al.* (2002a and 2002c). It was found that the total transmitted force is proportional to the acceleration of the actuator. Hence, force

feedback is equivalent to feeding back the actuator acceleration. This leads to the conclusion that force feedback control has the physical meaning of adding an "apparent" mass to the inertial actuator mass. In the experiments, the first resonance frequency was lowered to 8.75 Hz. Using higher gains, the system became unstable because of the phase lag introduced by the electronic components used in the experiment.

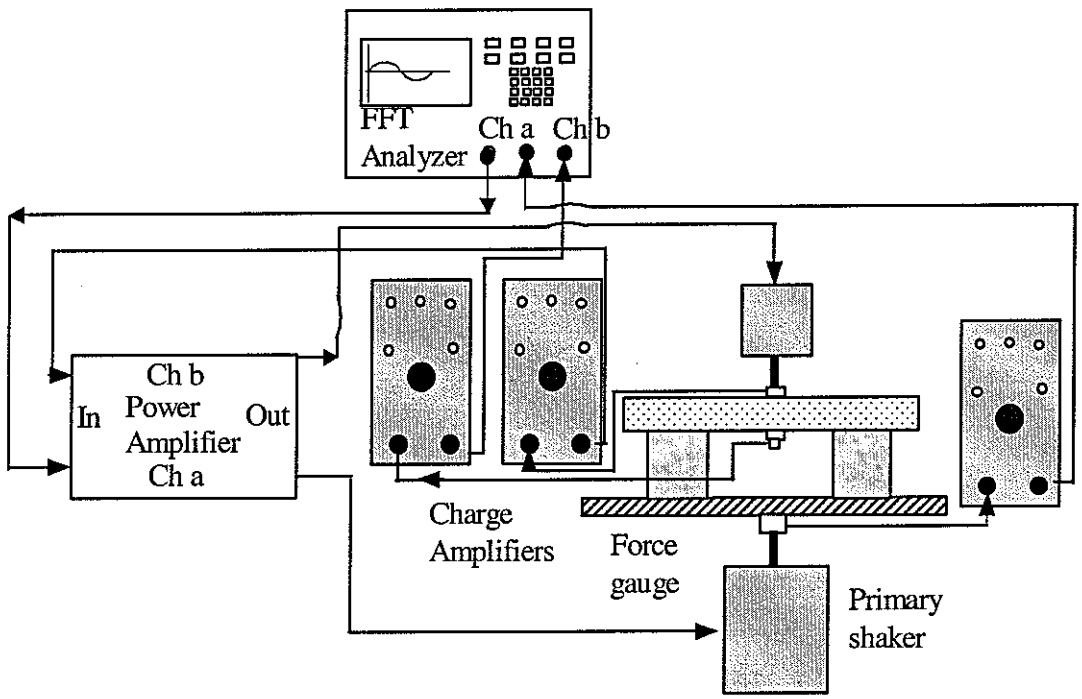

Figure 15. *Practical configuration in order to determine the equipment velocity per unit primary excitation when force feedback control is implemented.*

The corresponding simulation is plotted in Figure 18 (right). Since the ideal system is unconditionally stable, higher gains can be implemented and therefore the actuator resonance frequency can be lowered considerably. Also, since the Nyquist plot does not lie in the unit circle centred at (-1,0) as much as the measured one, smaller enhancement is predicted by the simulation at the equipment resonance.

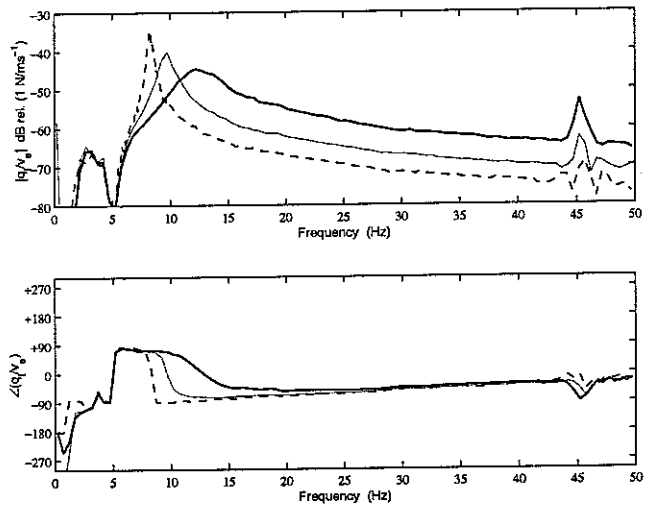

Figure 16. *Bode plot of the measured transfer function between equipment velocity and total measured force. Three force feedback gains h_f have been analysed: $h_f = 0$ (bold line), $h_f = 3$ (faint line), and $h_f = 10$ (dashed line).*

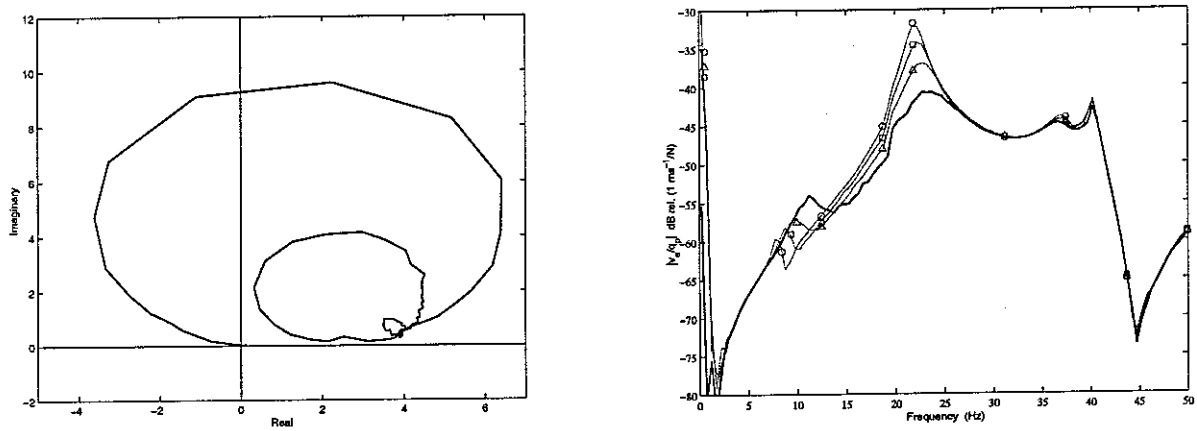

Figure 17. *Left: Nyquist plot of the treated measured plant response from secondary shaker input to force output. Right: treated measured velocity of the equipment per unit primary excitation. Results are shown for the passive system (control off, solid line) and for three values of feedback gain (faint lines): $h_f = 3$ (triangle), $h_f = 6$ (square), and $h_f = 10$ (circle). For gains greater than 10 the system was unstable.*

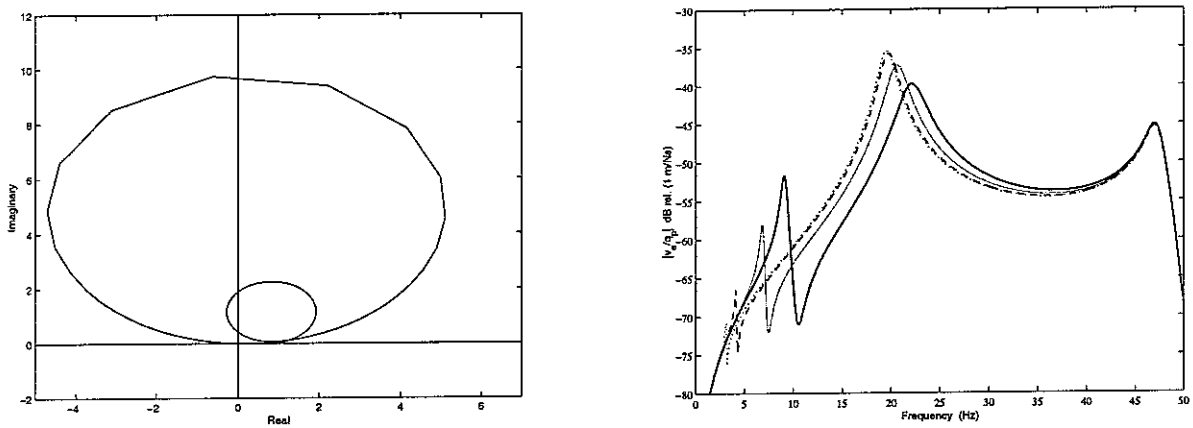

Figure 18. *Left: Nyquist plot of the simulated plant response from secondary shaker input to force output. Right: simulated velocity of the equipment per unit primary excitation. Results are shown for the passive system (control off, solid line) and for three values of feedback gain: h_f = 10 (faint line), h_f = 20 (dashed line), and h_f = 30 (dotted line). The ideal system is unconditionally stable.*

3.4 Integrated force feedback control

In this experiment, the same configurations as in section 3.3 were used in order to evaluate the stability properties and the performance of the closed loop system. The only difference was an ISVR-built integrator, which was used as a controller in the feedback loop before the power amplifier. This allowed the total transmitted force signal to be connected to the FFT analyser for measurement purposes, and also to be integrated within the feedback leg of the experimental set-up.

Figure 19 shows the total transmitted force to the equipment per unit equipment velocity. It can be noted that when the force feedback gain in increased, the inertial actuator resonance is damped.

The measured plant response, from secondary shaker input to integrated force output, for the active isolation system with the inertial actuator is shown in Figure 20 (left), which matches very closely the simulated response shown in Figure 21 (left). Compared to the previous case, the Nyquist plot appears rotated by 90° clock-wise. This is due to the effect of the integrator in the controller.

Also, despite the presence of low frequency causes of instability, the closed loop system is now significantly more stable than in the previous case. The spectrum of the measured

equipment velocity, normalized by the primary force, is shown in Figure 20 (right) with no control and with three values of feedback gain. The correspondent simulations are shown in Figure 21 (right). Also in this case, the theoretical findings match with the experimental measurements and in particular both effects on the first two resonances were experienced. Firstly, the magnitude of the inertial actuator resonance is attenuated. This damping effect was predicted and theoretically explained. Secondly, at the equipment resonance, the magnitude of the transfer function is greater then when no control is implemented (from this follows that an outer velocity feedback loop is needed in order to take energy away from the system), and its frequency lowered, as expected.

It was very difficult to increase the gain in such a way that it would set the closed loop system unstable. Such high gains were difficult to obtain with the power amplifiers in use. Most of the time, the power limit was reached before reaching the stability limit. This definitely showed how robust this solution is.

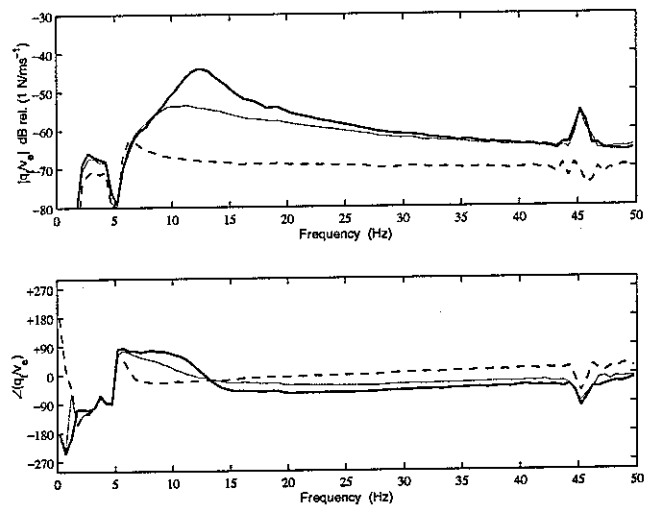

Figure 19. *Bode plot of the measured transfer function between equipment velocity and total measured force when the integrated force feedback scheme is implemented. Three force feedback gains h_{if} have been analysed: $h_{if} = 0$ (bold line), $h_{if} = 500$ (faint line), and $h_{if} = 2500$ (dashed line).*

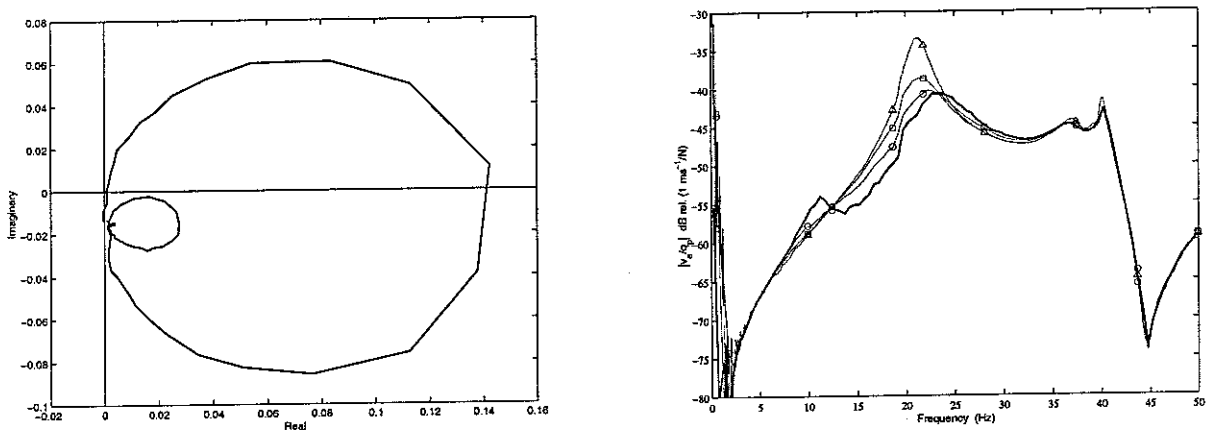

Figure 20. *Left: Nyquist plot of the treated measured plant response from secondary shaker input to integrated force output. Right: treated measured velocity of the equipment per unit primary excitation. Results are shown for the passive system (control off, solid line) and for three values of feedback gain (faint lines): h_{if} =500 (triangle), h_{if} = 1000 (square), and h_{if} = 2500 (circle). For gains greater than 2500 the system was still stable, but limitations due to the electronics occurred.*

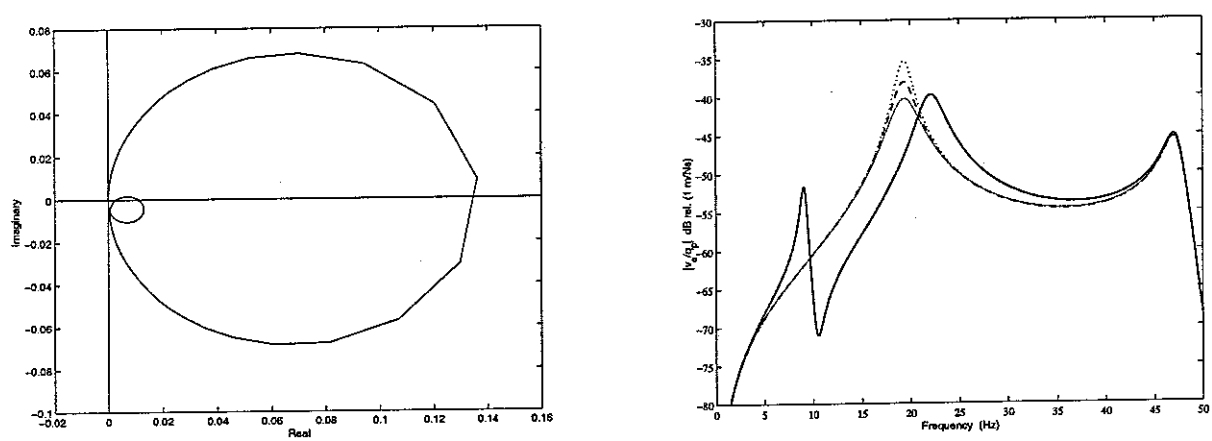

Figure 21. *Left: Nyquist plot of the simulated plant response from secondary shaker input to integrated force output. Right: simulated velocity of the equipment per unit primary excitation. Results are shown for the passive system (control off, solid line) and for three values of feedback gain: h_{if} =500 (faint line), h_{if} = 1000 (dashed line), and h_{if} = 2500 (dotted line).*

3.5 Force and velocity feedback control

In this case, the plant is considered to be the original plant with in addition the inner force feedback loop. In order to evaluate the stability properties of the closed loop system, white noise from the FFT analyser was used to drive the command signal (its definition can be found in Benassi *et al.*, 2002c). This signal was also connected to channel A of the analyser. When the equipment structure was excited, the acceleration signal at centre of the piece of equipment was measured via an accelerometer. The acceleration signal was then passed to a general signal conditioner and converted to a velocity signal by an integrated module inside the signal conditioner. The integrator was operated in conjunction with a high-pass filter, whose cut-off frequency was preset to be 1 Hz. Finally, the velocity signal was connected into channel B of the analyser to measure the frequency response function of the absolute equipment velocity per unit command signal. The inner loop was implemented using the signal from the force gauge underneath the inertial actuator. This signal was then connected to a signal conditioning box , amplified and then connected to the secondary shaker. An ISVR-built summing box was used to add the command signal (white noise in this case, while it was the amplified equipment velocity in the performance measurement) to the output of the signal conditioner which carried the total transmitted force information. Figure 22 shows a practical implementation of the experimental set-up, and Figure 24 (left) shows the Nyquist plot obtained from this measurement for different values of the inner gain.

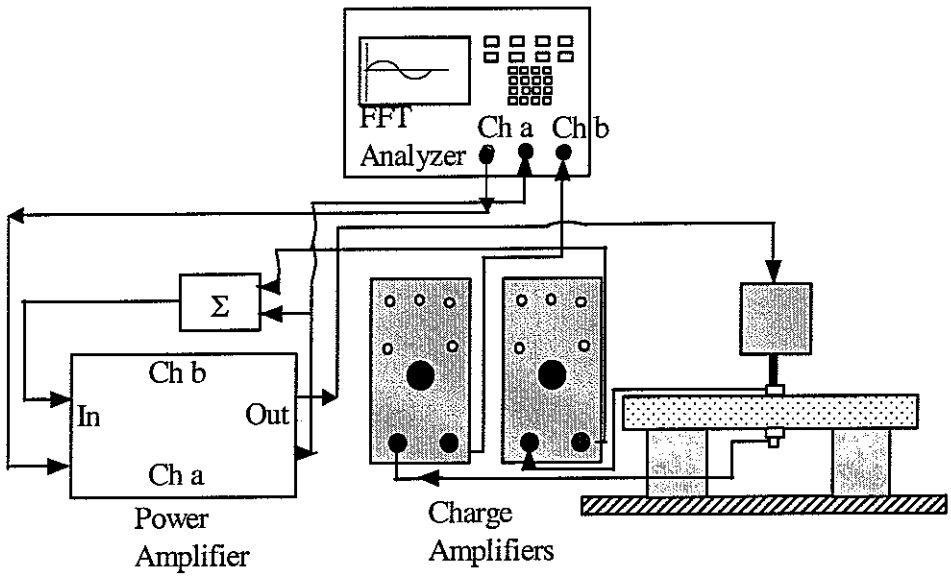

Figure 22. *Practical configuration in order to determine the equipment velocity per command signal.*

In order to evaluate the performance of the strategy described the set-up in Figure 22 was modified. The FFT analyser was used to measure the velocity response of the piece of equipment as well as generate the white noise signal. The white noise signal drove the primary shaker to excite the flexible base, and the excitation force signal was measured by a force transducer connected to channel A of the analyser. When the equipment structure was excited, the acceleration signal at centre of the piece of equipment was measured via an accelerometer. The acceleration signal was then passed to a general signal conditioner and converted to a velocity signal by an integrated module (operated in conjunction with a high-pass filter) inside the signal conditioner. The velocity signal was connected into channel B of the analyser to measure the frequency response function of the absolute equipment velocity per unit excitation force. A built-in filter in the analyser was employed to reduce aliasing. As explained in the above paragraph, the inner loop was implemented based on the measurement of the total transmitted force. Figure 23 shows a practical implementation of the experimental set-up, and Figure 24 (right) shows the experimental results.

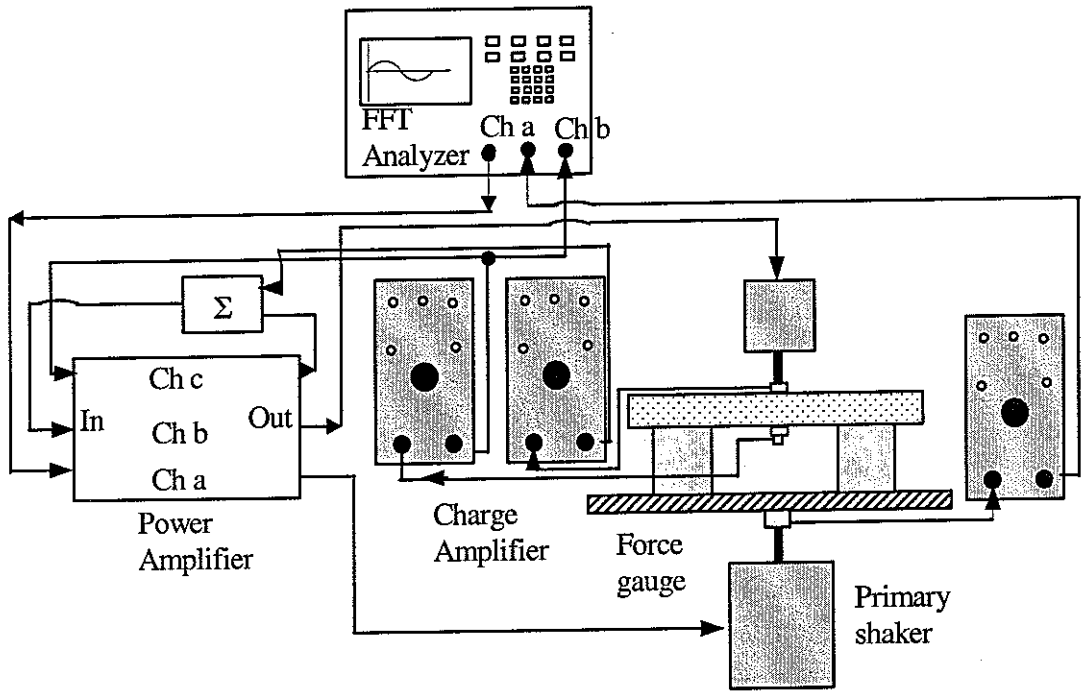

Figure 23. *Practical configuration in order to determine the equipment velocity per unit primary excitation when the force and velocity control scheme is implemented.*

The measured plant response, from command signal input to integrated accelerometer output, for the active isolation system with the inertial actuator is shown in Figure 24 (left), which is similar to the simulated response shown in Figure 25 (left). In this case, there is no primary disturbance arising from the base support and three Nyquist plots are shown for different inner force loop gains. The conclusion that can be drawn is that by increasing the inner loop gain, the closed loop system (when the outer loop is also implemented) gets closer to instability.

The spectrum of the measured equipment velocity, normalized by the primary force, is shown in Figure 24 (right) with no control and with three values of feedback gain. This can be compared to the theoretical simulations of Figure 24 (right). It can be noted that there is good agreement between simulations and theory, even if it must be taken into account the fact that in the simulation higher gains were used to show the potential of this scheme. Experimentally, an attenuation of the vibration at the mounted equipment resonance can be achieved using this arrangement, but some enhancement of the disturbance at the inertial actuator resonance frequency then occurs, as expected. This

enhancement increases rapidly if the velocity feedback gain (desired impedance) is further increased until the system becomes unstable. Some attenuation was also observed in the higher frequency base resonances with this system. The maximum measured attenuation is about 12 dB, and this is due to the unstable nature of the system at high gains. The performance plot was obtained by keeping the inner force feedback gain constant and varying the outer velocity feedback gain (desired impedance). The main effect of the inner loop is to lower the inertial actuator resonance frequency, while the main effect of the outer gain is to attenuate the magnitude of the equipment velocity. However, when the desired impedance is increased, enhancement of the response is experienced at the first resonance and this will eventually lead the overall system to instability.

Another main feature of this control strategy that was proven experimentally was that the inner force loop changes the system in such a way that velocity feedback gains that would drive the system unstable if only DVFB were implemented are now effective and work in the stable region. Also, the poor robustness of the inner loop, as described in section 3.3, tends to drive the system unstable even for small inner loop gains.

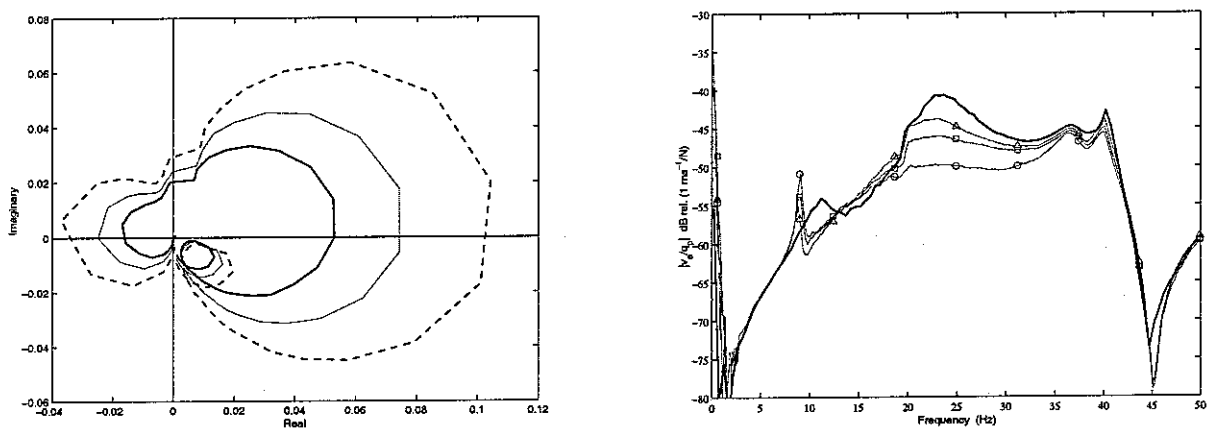

Figure 24. *Left: Nyquist plot of the treated measured plant response from command signal to integrated accelerometer output. Results are shown for three values of the force feedback gain: h_f =0.5 (solid line), h_f =1 (faint line), h_f = 2 (dashed line). Right: treated measured velocity of the equipment per unit primary excitation. Results are shown for the passive system (control off, solid line) and for three values of the velocity feedback gain (faint lines) when the force feedback gain was set to h_f = 6: Z_D =20 (triangle), Z_D = 30 (square), and Z_D = 50 (circle). For gains greater than 50 the system was unstable.*

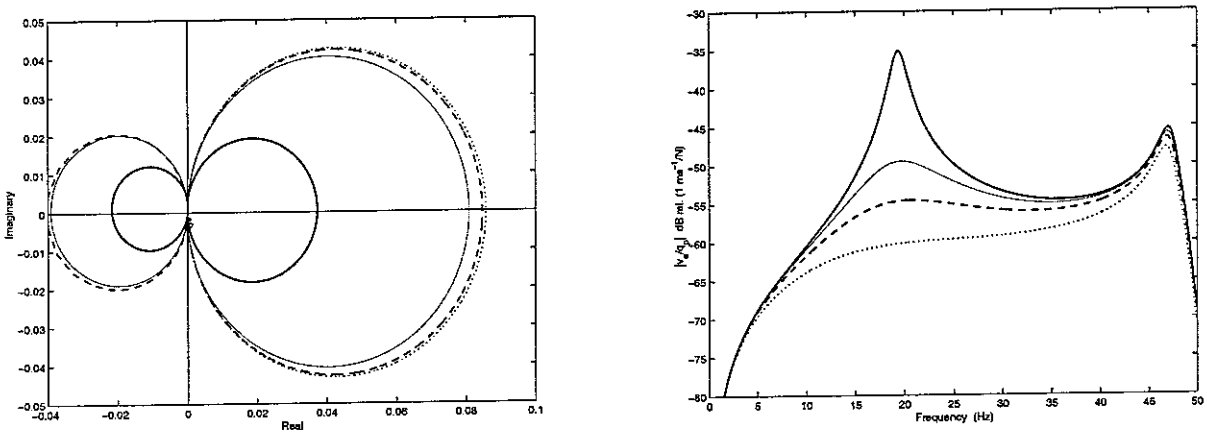

Figure 25. *Left: Nyquist plot of the simulated plant response from command signal to integrated accelerometer output. Results are shown for four values of the force feedback gain: h_f =0.5 (solid line), h_f =1 (faint line), h_f = 2 (dashed line), h_f = 10 (dotted line). Right: simulated velocity of the equipment per unit primary excitation. Results are shown for four values of the velocity feedback gain when the force feedback gain was set to h_f = 10: Z_D =0 (solid line), Z_D =20 (faint line), Z_D = 50 (dashed line), and Z_D = 200 (dotted line).*

3.6 Integrated force and velocity feedback control

The same configurations as in section 3.5 were used in this experiment in order to evaluate the stability properties and the performance of the closed loop system. The only difference was an ISVR-built integrator, which was used as a controller in the inner feedback loop before the power amplifier. This allowed the total transmitted force signal to be connected to the FFT analyser for measurement purposes, and also to be integrated within the feedback leg of the experimental set-up.

The measured plant response, from command signal to integrated force output, for the active isolation system with the inertial actuator is shown in Figure 26 (left), which matches closely the simulated response shown in Figure 27 (left). Despite the presence of low frequency causes of instability due to the electronics, the closed loop system is now more stable than in the previous case. The spectrum of the measured equipment velocity, normalized by the primary force, is shown in Figure 26 (right) with no control and with three values of feedback gain. The corresponding simulations are shown in Figure 27 (right). Also in this case, the theoretical findings match with the experimental measurements and in particular both effects on the first two resonances were experienced.

Firstly, the magnitude of the inertial actuator resonance is attenuated and slightly shifted to lower frequencies. This damping effect was predicted and theoretically explained. Secondly, at the equipment resonance, the magnitude of the transfer function is well attenuated, while at frequencies slightly greater than the second resonance a little enhancement is experienced, as predicted in Figure 27 (right).

Even in this case, it was very difficult to increase the outer loop gain in such a way that it would set the closed loop system unstable. Such high gains were difficult to obtain with the power amplifiers in use. Most of the time, the power limit was reached before reaching the stability limit. This definitely showed how robust this solution is. The maximum attenuation that was obtained was about 13 dB, but it must be noted that this does not represent a limit due to stability issues. This limit was reached because of the power limit of the audio amplifiers that were used during the experiments.

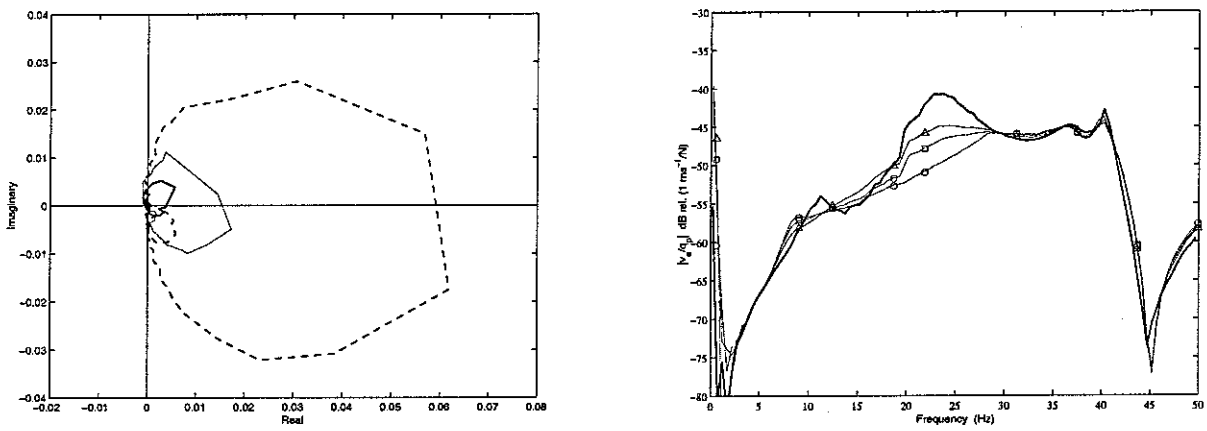

Figure 26. *Left: Nyquist plot of the treated measured plant response from command signal to integrated accelerometer output when an integrator is added within the inner loop. Results are shown for three values of the force feedback gain: h_{if} =20 (solid line), h_{if} =100 (faint line), h_{if} = 2500 (dashed line). Right: treated measured velocity of the equipment per unit primary excitation. Results are shown for the passive system (control off, solid line) and for three values of the velocity feedback gain (faint lines) when the force feedback gain was set to h_{if} = 2500: Z_D =30 (triangle), Z_D = 40 (square), and Z_D = 50 (circle). For gains greater than 50 the system was still stable, but limitations due to the electronics occurred.*

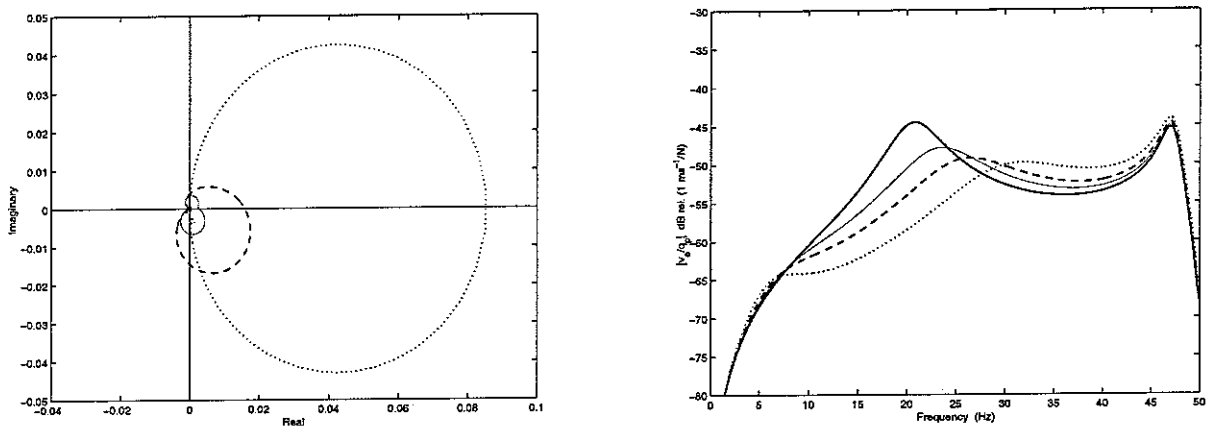

Figure 27. *Left: Nyquist plot of the simulated plant response from command signal to integrated accelerometer output when an integrator is added within the inner loop. Results are shown for four values of the force feedback gain: h_{if} =20 (solid line), h_{if} =100 (faint line), h_{if} = 5000 (dashed line). Right: simulated velocity of the equipment per unit primary excitation. Results are shown for four values of the velocity feedback gain when the force feedback gain was set to h_{if} = 1000: Z_D =0 (solid line), Z_D =30 (faint line), Z_D = 50 (dashed line), and Z_D = 200 (dotted line).*

3.7 Phase-lag compensator and velocity feedback control

The same configurations as in section 3.5 were used in this experiment in order to evaluate the stability properties and the performance of the closed loop system. The only difference was a passive phase-lag compensator designed and built by the first author (R_1 = 720 kΩ, R_2 = 72 kΩ, C = 0.1 μF), which was used as a controller in the inner feedback loop before the power amplifier. This allowed the total transmitted force signal to be connected to the FFT analyser for measurement purposes, and also to be integrated within the feedback leg of the experimental set-up.

The measured plant response, from command signal to integrated force output, for the active isolation system with the inertial actuator is shown in Figure 28 (left), which matches the simulated response shown in Figure 29 (left). Despite the presence of low frequency causes of instability due to the electronics, the closed loop system is now more stable than in the force and velocity feedback scheme. However, since the Nyquist plot is not entirely on the right hand side of the imaginary axis and portions of it intersect the negative part of the x-axis, instabilities are likely to happen at very high outer loop gains. Unfortunately, with the given electronic components it was not possible to push the system to its stability limit, even if using an appropriate combination of the gain values,

the system was behaving very close to instability. Also, it can be noted, as predicted by the simulations, that by increasing the inner loop gain h_{pl}, the stability properties of the overall feedback system improve. The spectrum of the measured equipment velocity, normalized by the primary force, is shown in Figure 28 (right) with no control and with three values of feedback gain. The corresponding simulations are shown in Figure 29 (right). Also in this case, the theoretical findings match with the experimental measurements and in particular both effects on the first two resonances were experienced. In fact, below the second cut-off frequency of the phase-lag compensator (22 Hz), the systems behaves as if integrated force and velocity feedback control was implemented, whereas at frequencies higher than 22 Hz, the system behaves as if force and velocity feedback control was implemented. As a result, the magnitude of the inertial actuator resonance is attenuated and slightly shifted to lower frequencies and at the equipment resonance, the magnitude of the transfer function is well attenuated, while at frequencies slightly greater than the second resonance no enhancement is experienced, unlike the case discussed in Section 3.6. Even in this case, it was very difficult to increase the outer loop gain in such a way that it would set the closed loop system unstable. Such high gains were difficult to obtain with the power amplifiers in use. Especially for high values of the inner gain, the power limit was reached before reaching the stability limit. This definitely showed how robust this solution is, but it also shows the limitations of a passive phase-lag compensator. Adding an internal gain to the compensator through a set of operational amplifiers could solve this problem. Anyway, the maximum attenuation that was obtained was about 14 dB, but it must be noted that this does not represent a limit due to stability issues.

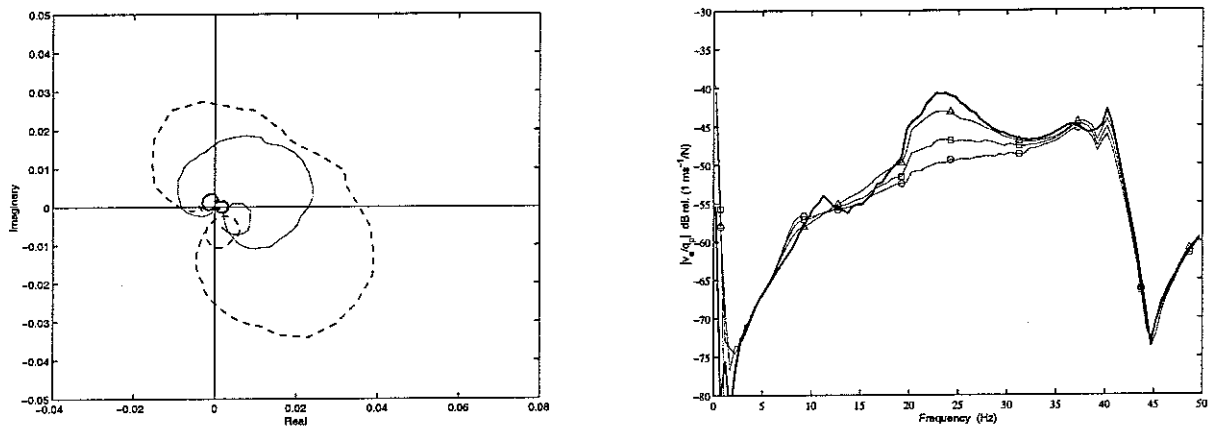

Figure 28. *Left: Nyquist plot of the treated measured plant response from command signal to integrated accelerometer output when a phase-lag compensator is added within the inner loop. Results are shown for three values of the force feedback gain: h_{pl} =20 (solid line), h_{pl} =100 (faint line), h_{pl} = 2500 (dashed line). Right: treated measured velocity of the equipment per unit primary excitation. Results are shown for the passive system (control off, solid line) and for three values of the velocity feedback gain (faint lines) when the force feedback gain was set to h_{pl} = 2500: Z_D =20 (triangle), Z_D = 40 (square), and Z_D = 50 (circle).*

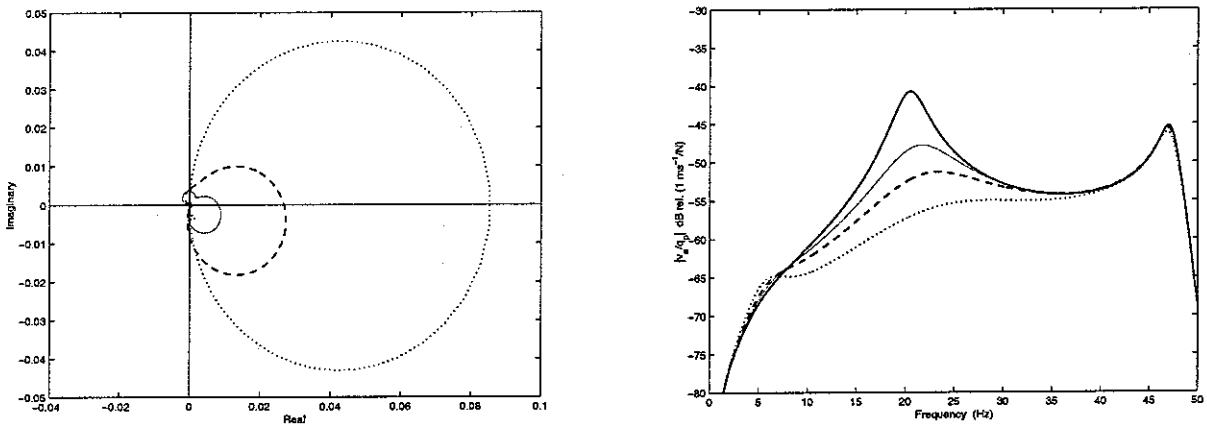

Figure 29. *Left: Nyquist plot of the simulated plant response from command signal to integrated accelerometer output when an integrator is added within the inner loop. Results are shown for four values of the force feedback gain: h_{pl} =20 (solid line), h_{pl} =100 (faint line), h_{pl} = 100,000 (dashed line). Right: simulated velocity of the equipment per unit primary excitation. Results are shown for four values of the velocity feedback gain when the force feedback gain was set to h_{pl} = 1000: Z_D =0 (solid line), Z_D =40 (faint line), Z_D = 50 (dashed line), and Z_D = 200 (dotted line).*

4. CONCLUSIONS

The objective of this work was to investigate the active isolation of a two-mount flexible equipment structure from a vibrating base structure using an inertial actuator. The dynamics and control mechanisms of the mounted rigid equipment structure on a flexible base plate have been studied experimentally and the results have been compared to the theoretical findings previously obtained. The equipment velocity responses measured from the experiments agree reasonably well with the predicted results, which demonstrates that the theoretical model can be used to help to understand the dynamics of the overall system. Good stability properties of the single- and multi-channel feedback control system are verified in the experimental implementations.

It was found from the simulations and the experiments that from a stability point of view, the force and velocity feedback control scheme does not guarantee a good stability margin at low frequency. This is especially true when the outer velocity gain is increased. On the other hand, from a performance point of view, this scheme offers very good results using lower power than the other schemes.

When an integrator is added to the system, the overall system significantly improves its stability characteristics. On the other hand, if high performance is needed, very high gains are necessary and therefore a lot of power is consumed.

The idea then to use a phase-lag compensator within the inner loop and a velocity feedback outer loop seems to be very attractive. In fact, simulations and experiments show that a strong reduction of the equipment resonance can be achieved, together with very good stability limits.

APPENDIX A: Geometrical and physical characteristics of the experimental set-up

This appendix contains the geometrical and physical characteristics equipment used during the experimentation work presented in this Technical Memorandum.

Parameter	Value
Material	Aluminium
Plate dimensions	0.2 x 0.1 x 0.018 m
Density	2700 kg/m^3
Young's modulus of elasticity	7.1e10 N/m^2
Shear modulus of elasticity	2.4e10 N/m^2
Poisson's ratio	0.33
Mass of the plate	1.08 kg
Moment of inertia of the receiver	1.4e-2 kgm^2

Table A1. *Geometrical and physical characteristics of the receiver.*

Parameter	Ring of rubber
External diameter	60 mm
Internal diameter	40 mm
Height	60 mm
Area	1.57e-3 m^2
Moment of inertia	5.1e-7 m^4
Density	909 kg/m^3
Young's modulus of elasticity	8e5 N/m^2
Shear modulus of elasticity	2.7e5 N/m^2
Poisson's ratio	0.3

Table A2. *Main characteristics of the rubber mounts.*

Parameter	Value
Moment of inertia	1.4e10^{-2} kgm^2
Total stiffness of each mount	24093 N/m
Total viscous damping for each mount	17.94 Ns/m
Effective mount damping ratio	4.8 %
Distance between mounts	134 mm

Table A3. *Summary of the passive properties of the isolators (mounts).*

Parameter	Value
Material	steel
Dimensions	700 x 500 x 2 (mm)
Damping ratio	0.01

Table A4. *Summary of the physical and geometrical properties of the base*

Mode	Experimental frequency (Hz)	Calculated frequency (Hz)
(2,0)	32.6	44.8
(2,1)	41.7	49.0
(2,2)	58.8	65.4
(2,3)	91.1	98.8
(3,0)	100.0	123.3
(3,1)	105.0	129.2
(3,2)	128.0	149.8
(2,4)	139.0	151.8
(3,3)	166.2	186.0

Table A5. *First 9 modes of the base supporting plate.*

Specification	Value
Total mass	0.91 kg
Maximum sine force – peak	8.9 N
Max displacement pk-pk (DC)	2.5 mm
Max sine velocity – peak	1.31 m/s
Max sine acceleration – pk	1373 m/s^2
Suspension axial sfiffness	3.15 N/mm
Electrical requirement – Amplifier	0.09 kVA
Impedance at 500 Hz	3 Ω

Table A6. *Specifications for a single control shaker LDS type V101.*

Specification	Value
Maximum sine force – peak	196 N
Useful frequency range	DC to 9 kHz
Maximum displacement	±8.8 mm
Maximum acceleration	981 m/s^2
Maximum input power	100 VA
Maximum working current	9 A

Table A7. *Specifications for a single control shaker LDS type V403.*

	Measurements		Model	
Modes	Without Isolator	With Isolator	Without Isolator	With Isolator
(2,0)	32.2	39.8	44.8	48.5
(2,2)	58.8	63.1	65.4	70.4
(2,4)	139.9	145.2	151.8	153.5
(4,0)	225.9	226.0	241.7	241.9

Table A8. *Base plate modes observed by measurements and by simulations with and without the effect of the active isolator system.*

Equipment	Type
Accelerometer	B&K 4375
Force gauge	B&K 8200
Charge amplifier	B&K 2635
Power amplifier	HH Electronics MOS-FET
Integrator	ISVR designed
FFT Servo Analyzer/Generator	Advantest R9211B/C
Primary Shaker	LDS 403
Secondary shaker	LDS 101
Current meter	3 A and 5 A
Summing Box	ISVR designed

Table A9. *List of the equipment*

References

Ananthaganeshan, K. A., Brennan, M. J., and Elliott, S. J., 2001, "Low and High Frequency Instabilities in Feedback Control of a Vibrating Single Degree of Freedom System," ISVR Technical Report No. 870.

Benassi, L., Gardonio, P., and Elliott, S.J., 2002a, "Equipment Isolation of a SDOF System with an Inertial Actuator using Feedback Control Strategies – Part I: Theory," ISVR Technical Memorandom No. 883, University of Southampton.

Benassi, L., Gardonio, P., and Elliott, S.J., 2002b, "Equipment Isolation of a SDOF System with an Inertial Actuator using Feedback Control Strategies", *Proceedings of the ACTIVE 2002Conference, Southampton, U.K.*, 15-17 July 2002.

Benassi, L., Gardonio, P., and Elliott, S.J., 2002c, "Equipment Isolation of a SDOF System with an Inertial Actuator using Double Feedback Control Strategies", ISVR Technical Memorandom No. 893, University of Southampton.

Brüel & Kjær, Piezoelectric Accelerometers and Vibration Preamplifiers – Theory and Application Handbook.

Elliott, S. J., Serrand, M., and Gardonio, P., 2001, "Feedback Stability Limits for Active Isolation Systems with Reactive and Inertial Actuators," J. Vibration and Acoustics, Vol. 123, April 2001, pp. 250-261.

Gardonio, P., Elliott, S. J., and Pinnington, R. J., 1996, "User Manual for the Isolating System with two Active Mounts Constructed at ISVR for the ASPN Project Final Experiment," ISVR Technical Memorandom No. 801, University of Southampton.

Gardonio, P., Elliott, S. J., and Pinnington, R. J., 1997a, "Active Isolation of Structural Vibration on a Multiple-Degree-of-Freedom System, Part I: the Dynamics of the System," J. Sound and Vibration, **207**, No. 1, pp. 61-93.

Gardonio, P., Elliott, S. J., and Pinnington, R. J., 1997b, "Active Isolation of Structural Vibration on a Multiple-Degree-of-Freedom System, Part II: Effectiveness of Active Control Strategies," J. Sound and Vibration, **207**, No. 1, pp. 95-121.

Karnopp, D., 1995, "Active and Semi-active Vibration Isolation," ASME J. Mech. Des., **117**, pp. 177-185.

Kim, S. M., Elliott, S. J., and Brennan, M. J., 1999, "Active Vibration Isolation of a 3-Dimensional Structure using Velocity Feedback Control," ISVR Technical Memorandum No. 845.

Leissa, A. W., 1969, *Vibration of Plates*, NASA SP-160.

L.D.S., Installation and Operating Manual for the V100 Series Vibrators. Manual No. 899061, 2nd Edition.

L.D.S., Installation and Operating Manual for the V400 Series Vibrators. Manual No. 586441, 1st Edition.

Ren, M. Z., Seto, K., and Doi, F., 1997, "Feedback Structure-Borne Sound Control of a Flexible Plate with an Electromagnetic Actuator: the Phase Lag Problem," J. Sound and Vibration, **205**, No. 1, pp. 57-80.

Serrand, M., 1998, "Active Isolation of Base Vibration," MSc thesis, University of Southampton.